LETTER TO THE EDITOR

Long-range correlations in smoke-particle aggregates

S R Forrest† and T A Witten Jr‡

Randall Laboratory of Physics, University of Michigan, Ann Arbor, Michigan 48109, USA

Abstract. Ultrafine smoke particles stick together to form chain-like aggregates. We find that the particle density has long-range correlations of the same form in iron, zinc or silicon dioxide aggregates. The correlation data suggest a power-law spatial dependence giving a Hausdorff dimension between 1·7 and 1·9. We discuss the consistency of these results with a model based on percolation. We also compare our results with a random-walk model, which has a nominal Hausdorff dimension of 2.

1. Introduction

Certain extended physical systems (Fisher 1974) such as a fluid near its critical point have a fluctuating density $\rho(r)$ whose spatial correlations extend to arbitrarily long distance. In such cases the correlations typically obey a characteristic power law

$$\langle \rho(r)\rho(0)\rangle - \langle \rho(0)\rangle^2 \propto r^{-A} \tag{1}$$

over a large range of r. The exponents A in such power laws often have two striking features. First, in contrast to most power laws one encounters, A is usually not a simple fraction arising from dimensional considerations: it is 'anomalous'. Second, A is typically unaffected by a continuous alteration of the parameters of the system: it is 'universal'.

Recently 'anomalous' exponents like A have been discovered in a remarkably broad range of physical systems. The best known examples are extended matter at a second-order phase transition such as the liquid–gas critical point mentioned above. Here the observed power laws are manifestations of a symmetry known as the renormalisation group. This is a type of covariance of the system under spatial dilation. Long polymers (McKenzie 1976), the spin glass (Harris *et al* 1976) and connected clusters in a system near its percolation threshold (Kasteleyn and Fortuin 1969) appear to have 'critical' correlations in complete analogy to second-order phase transitions. Critical-point behaviour of a more general sort is thought (Mandelbrot 1977) to occur in the velocity autocorrelations of strongly turbulent fluids (Nelkin 1975, Abarbanel 1978), in the star density profile within star clusters and even in the spatial conformation of coastlines (Mandelbrot 1977).

We have observed that aggregates of ultrafine smoke particles can have long-range density correlations. Further, these correlations appear to have a characteristic exponent A which is both 'anomalous' and 'universal'. In the systems we have studied,

the smoke particles condense from the vapour produced by a hot filament or flame in a cool, dense gas (Wada 1967). The particles—approximately 40 Å in radius—stick together to form chain-like aggregates containing several thousand particles. Figure 1 shows an electron micrograph of a typical aggregate of Fe particles. Such particle aggregates have been observed in many studies of small metal particles (see, for
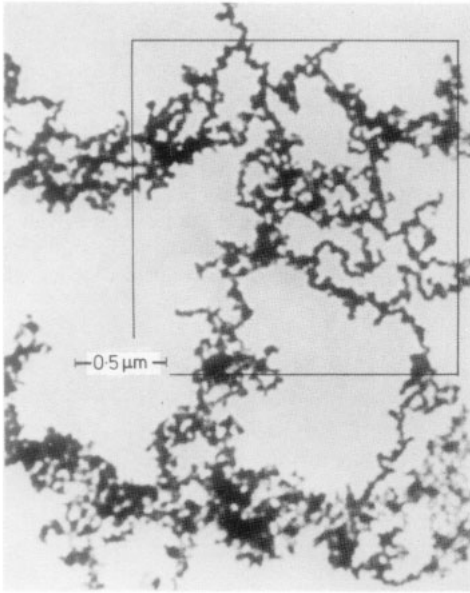
(a)
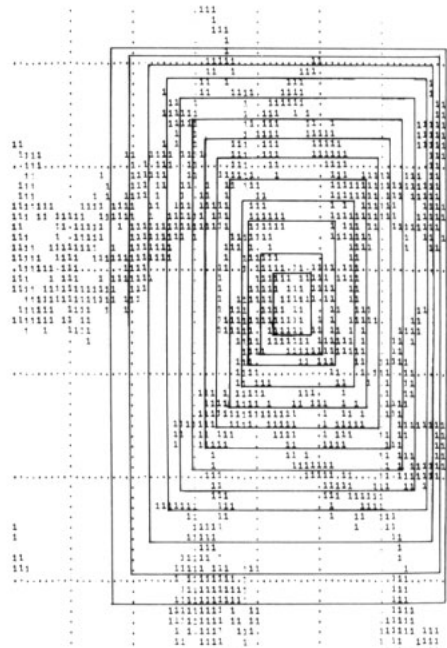
(b)
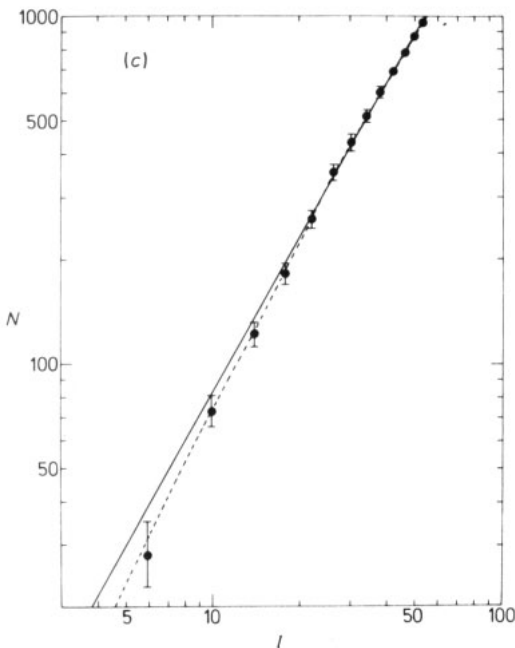
(c)

Figure 1. (a) Transmission electron micrograph of the iron aggregate used for image 2. The actual aggregate is many times larger than the segment shown. Constituent particles are roughly 35 Å in radius. The box corresponds to the outer box on the digitised image (b). (b) A segment of the digitised image of (a). The series of boxes used to generate the data of (c) are shown. The boxes do not appear as squares because of the format of the computer printer. (c) Result of a typical point count. Each data point corresponds to a box in Fig. 1b, where N is the number of 1's counted in a box of side l. The line, of slope $D = 1.51 \pm 0.05$, is a least squares fit to the data weighted according to the number of 1's in a given box. Several similar sets of counts are made at random starting locations on the image to determine the D quoted in table 2. The error bars ($= \sqrt{N}$) indicate the relative weight given to the various data points in fitting to a straight line. The broken line represents a least squares fit of the data to the form: $N = Al^D e^{-l/l_0} + Bl^2$ where $D = 1.90 \pm 0.05$ and $l_0 \sim 100$.

example, Granqvist and Buhrman 1976). By measuring the density of particles as a function of position, we may determine the density autocorrelation function $\langle \rho(r)\rho(0) \rangle$. In several samples of iron, zinc and silicon dioxide aggregates produced under widely different conditions we found that the density profiles had power correlations as in equation (1) with A between 0·1 and 0·3.

In the analysis of our smoke-particle aggregates we employ the language of the Hausdorff dimension (Hausdorff 1919, Mandelbrot 1977) which is a convenient method of describing physical systems having dilation symmetry (Stanley *et al* 1976). An infinite set of points in space is said to have Hausdorff dimension less than or equal to D if it can be covered by $O(a^D)$ balls of radius a in the limit $a \to 0$. Such a set (in d-dimensional space) has density correlations of a power-law type with the exponent A equal to $d - D$.

2. Experimental results

We have analysed the density distribution in five different samples of aggregates, numbered 2–6. Samples 2–5, containing iron or zinc particles, were made in our laboratory by the procedure outlined below. Micrograph 6, obtained from a Cabot Corporation brochure (*Cabot Corporation* 1975†) showed aggregates of their 'Cab-O-Sil' powder. This commercial substance consists of SiO_2 particles produced in a flame process.

Figure 2 shows the apparatus used to make the iron and zinc aggregates. A 0·013 cm daimeter tungsten wire electroplated with iron or zinc is rapidly heated by a short (250 ms) current pulse so that the plated metal vaporises. A dense gas (10^{-3} to
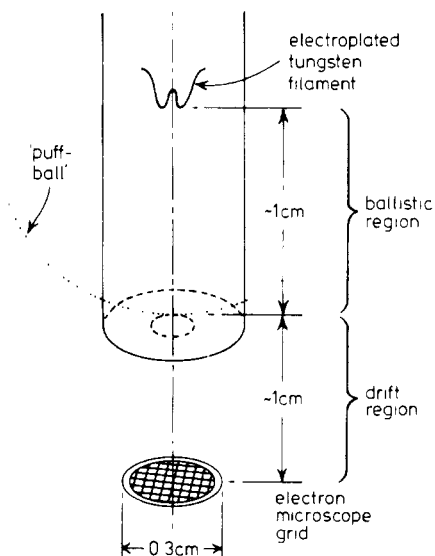

Figure 2. Schematic diagram of experimental apparatus used for production of metallic particle aggregates. The assembly is contained in a metal can with plumbing to admit helium gas. The can may be immersed in liquid nitrogen or helium.

10^{-1} of atmospheric number density) of helium confines the metal vapour so that it condenses into crystallites in a region close to the filament. These crystallites are the particles which make up our aggregates. They are roughly spherical and uniform in size, the mean radius being 35 Å, with a standard deviation of 15 Å, as determined via electron microscopy measurements.

The hot particles at first move rapidly away from the filament, but they soon come to rest in the gas ambient due to collisions with the gas atoms. The stopping distance for the different particles is nearly the same, and thus a thin spherical shell region with a high density of crystallites forms roughly 1 cm from the filament. The radius of the shell, or 'puff-ball' depends on the gas density: higher density makes a smaller puff-ball. It is in the puff-ball region that the particles stick together to form the aggregates we observe. The aggregates tend to be larger for higher gas temperature, and also when the puff-ball is smaller. Once formed, the aggregates settle slowly onto an electron microscope grid, which we later examine.

By placing electron microscope grids at various distances from the filament, we have determined that most of the aggregation occurs in the high-density puff-ball region, and that the aggregates do not change noticeably in size or shape even when allowed to fall distances of 3 cm or more. We have studied aggregates produced at widely varying temperatures and gas densities. We find that both iron and zinc have an equal ability for form chains under all conditions, in disagreement with observations made by Granqvist and Buhrman (1976). Thus magnetic forces do not play a dominant role in aggregate formation in our experiments.

Table 1 lists the five micrographs we have analysed in this study, along with the conditions under which they were made. The silicon dioxide is produced by the hydrolysis of silicon tetrachloride vapour in a flame of hydrogen and oxygen (*Cabot Corporation* 1975). The resulting aggregates are then allowed to cool and settle. We produced the first four samples under conditions favourable for forming many large aggregates; indeed, the connected aggregates extended far beyond the boundaries of the photographs. Only those that tended to lie flat on the microscope grid were photographed, as the depth of field of the transmission electron microscope is severely limited.

Next, each photograph was digitised by hand to produce a matrix of 'ones' and 'blanks' as shown in figure 1(*b*), the 'ones' ('blanks') corresponding to the presence (absence) of a particle. We analysed the digitised images with a computer in two different ways. The first method was motivated by the Hausdorff dimension approach of Mandelbrot (1977). A centre point on the image was picked at random, and then a

Table 1. Sample preparation.

Image matrix	Material	Gas density (cm^{-3})	Gas temperature (K)	Area of electron micrograph (μm^2)
2	Fe	$8 \cdot 1 \times 10^{17}$	295	9·2
3	Fe	$7 \cdot 3 \times 10^{16}$	77	3·1
4	Zn	$3 \cdot 2 \times 10^{17}$	77	7·7
5	Zn	$3 \cdot 2 \times 10^{17}$	77	7·7
6	SiO$_2$	—	—	1·2

series of nested squares of different sizes was placed around it and the number of 'ones' in each square counted. This analysis, performed on a set of points with a Hausdorff dimension, would yield a power-law relationship between the length l of the square and the number of points N within it, namely $N \propto l^D$. For our images, we also obtained a power-law relation, with D varying in the range 1·5 to 1·6 with l varying over a factor-of-forty range in most cases. We found that our results were most reproducible when squares were chosen whose centres of mass coincided with their geometric centres. A typical series of such squares is shown in figure 1(b). Thus the computer would begin by defining at random a large square on the image, finding the centre of mass of the points within it, and moving the square until the centre of mass and the geometric centre coincided. Then the number of points inside was counted. Next a slightly smaller square was chosen concentric with the previous one. It was moved until its geometric centre and its centre of mass coincided, and so on. If the process resulted in a square being moved off the image or outside the previous square, the series was terminated. A value of D was computed for each series by least-squares fitting $\ln N$ against $\ln l$ to a straight line. In this weighted fit we assumed that as N increased, the relative uncertainty in N decreased roughly as $N^{-1/2}$. We verified the accuracy of this procedure by analysing a mathematical Hausdorff set known as a Koch curve (see, e.g., Mandelbrot 1977) with $D = \ln 3/\ln 2$. Our measuring method gave the correct D to within 1%—well within our statistical uncertainty (see table). We also analysed an image of points placed at random, and obtained the expected exponent, $D = 2$, to the same order of precision.

The accuracy of our method is limited by the finite total number of points in the image analysed; we have verified that the statistical variations in our measured exponents decrease when there are more points in the image. Another limitation on our precision arises from the finite size of our image. It is because of this finite size that our data span only a limited range of l.

We obtained results comparable with these by our second method of analysis, in terms of the density autocorrelation function. In this method we found the average density of occupied points in the digital image at a distance r from each occupied point, and this was done for all values of r (see figure 3(a)). In a set of points with a Hausdorff dimension, this average density should fall off with distance as r^{D-d}. Values of D for each image were found by plotting the logarithm of the average density against $\ln r$. Then D was obtained from the initial slope, as determined by equally weighted least-squares fitting. The errors quoted in table 2 give the range of D values whose χ^2 lay within a factor two of the minimum.

We verified the accuracy of this method using Koch curves and random images, as with our first method. We found that our results were reliable for distances r less than about a third of the image size. For larger distances the correlation function varied widely and depended sensitively on, for example, the size and location of the region sampled. These variations are due to the large, strongly correlated statistical fluctuations commonly encountered in correlation functions sampled over a region not much larger than the distance r (Jenkins and Watts 1968). We verified this idea by analysing a series of images, each with a Koch curve in a random position and orientation. These images were approximately the same size as our smoke images, and the Koch curves had $D = \ln 3/\ln 2 = 1·59$. If these images had been infinite, all would have had identical correlation functions. In the actual images the measured correlations fluctuate somewhat from image to image, and this gives a crude measure of the statistical uncertainties inherent in the sampling method. As in our smoke images, these fluctuations were
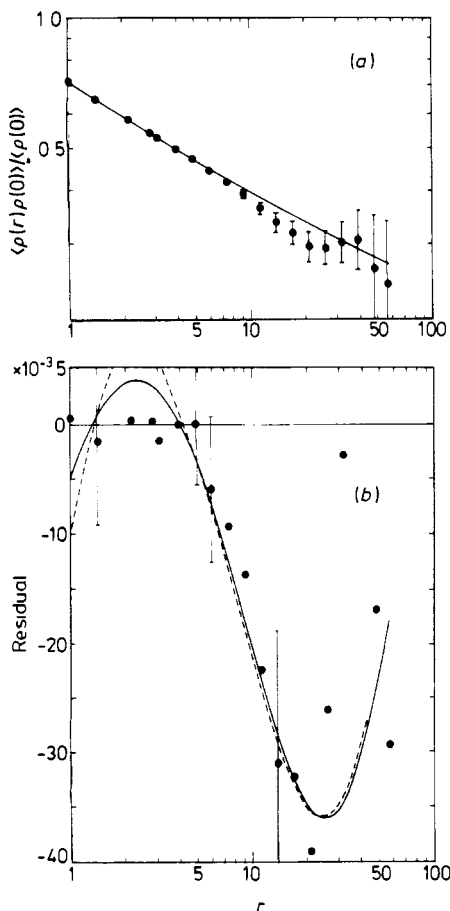
Figure 3. (*a*) Log–log plot of density autocorrelation divided by average density against distance *r* for the digitised image of figure 1(*b*). Unit of length is array element length in figure 1(*b*). The curve is of the form $Ar^{1\cdot695-2}+B$, where the exponent, *A* and *B* were adjusted for a least-squares fit to the first four data points to obtain the initial slope. Error bars shown were obtained from the Koch curve study (see text). (*b*) Deviation of the data points from the line in (*a*) (horizontal line at 0). The full curve is of the form $Ar^{1\cdot695-2}\exp(-r/15\cdot8)+B$, where *A* and *B* were adjusted for a least-squares fit to the first 14 points. The broken curve is of the form $AK_0(r/15\cdot8)+B$, where K_0 is the modified Bessel function.

highly correlated from point to point, so that one cannot infer the statistical uncertainties from the scatter of the data in a single image. We have assigned errors to our data points assuming that the relative error for a given distance *r* was the same as the relative spread of the data at that *r* in the Koch curve series. The error bars in figure 3 were drawn using this rough estimate.

We have summarised the results of these two methods in table 2. For each image we have listed the measured exponent *D*, with its statistical uncertainty, as obtained by each method. We have also indicated the approximate range of distance *r* sampled in each case. The exponent *D* for all these cases lies in the range 1·5 to 1·7. The exponents obtained by the point-counting method are systematically lower than those obtained from the density correlation method. We believe this is due to the breakdown of our power-law correlations in favour of an exponential decrease at large distances. Indeed, some type of exponential decrease is expected in an extended matter system for sufficiently large *r* (see, e.g., Duneau *et al* 1974). The effect of the exponential is to reduce the apparent *D* at large distances. The square-counting method weights the larger distances more heavily than does the correlation function method. Thus any exponential fall-off effects would cause the counting method to result in a smaller *D*, as we observe. We also see evidence for a more rapid fall-off at large distances by looking

Table 2. Measurements of D.

Image matrix	Dimensions digitised image matrix	No of 'ones' in digitized image	Apparent D			
			Point counting[a]		Density auto-correlation[b]	
			$N \propto L^D$	$N \propto L^D \times \exp(-L/r_0)$	D	Range of r fitted
Real images						
2	70×96	1419	$1\cdot52 \pm 0\cdot04$	$1\cdot90 \pm 0\cdot05$	$1\cdot69 \pm 0\cdot02$	1–12
3	97×120	2149	$1\cdot56 \pm 0\cdot02$	$1\cdot90 \pm 0\cdot05$	$1\cdot68 \pm 0\cdot01$	1–12
4	96×120	1797	$1\cdot50 \pm 0\cdot04$	$1\cdot85 \pm 0\cdot05$	$1\cdot67 \pm 0\cdot02$	1–7
5	94×119	2934	$1\cdot60 \pm 0\cdot04$	$1\cdot85 \pm 0\cdot05$	$1\cdot68 \pm 0\cdot02$	1–13
6	50×49	523	$1\cdot55 \pm 0\cdot06$[c]	$1\cdot85 \pm 0\cdot05$	$1\cdot55 \pm 0\cdot02$	1–5·5
Test images						
Koch ($D = 1\cdot5850$)	79×77	2375	$1\cdot57 \pm 0\cdot02$		$1\cdot55 \pm 0\cdot02$	1–13
Random ($D = 2$)	100×100	2020	$2\cdot06 \pm 0\cdot02$		$2\cdot00 \pm 0\cdot01$	1–30

[a] Uncertainties are the standard deviations of fits to counts originating at several random sites on the image. The range of l in these fits was roughly 2–80.
[b] Obtained by least-squares fit to a straight line on a log–log plot. The points spanning the range of r values indicated were equally weighted. Errors quoted are the nominal statistical errors of the fitted slope.
[c] Range of l samples was 2–50.

at our power-law fits. There is often a slight downward curvature in our log–log plots. If we include exponential fall-off effects in our fitting, the fit to the data improves and the D values increase as expected. For fitting the correlation data we chose the functional form $\langle \rho(r)\rho(0) \rangle = Ar^{D-2} \exp(-r/r_0) + B$ where A, B, D and r_0 are fitted parameters. A corresponding form for the point count N as a function of the box size l is $N = A'l^D \exp(l/l_0) + B'l^2$. Here B and B' reflect the magnitude of the random background on our data, and r_0 and l_0 are characteristic length scales. Column 5 of table 2 reports the D values obtained using this fitting in the point-counting method. The nominal errors are based on the variations in D noted when several sets of data on a given image were approximately fitted. The broken line in figure 1(c) illustrates the improvement of the fits when the exponential fall-off was included. The l_0 values were typically about double the largest l value for each set of data. Evidently these data suggest an exponential fall-off, but they are also compatible with no such fall-off. The D values vary significantly depending on which functional form is chosen. The range of D values thus obtained overlaps the values from the correlation function method. The correlation function data may also be treated assuming exponential fall-off, as figure 3(b) illustrates. In this figure, we plot the residuals of the data from the line in figure 3(a). The full curve is the fit when exponential fall-off is included. Again the fit improves for large r, but the D values, taken from the initial slope, do not change significantly.

3. Discussion

Our results, though not conclusive, suggest that the particle distribution in these random aggregates arises from some type of critical process. For comparison we list in

table 3 the D values which emerge in some model systems. One possible model for our system is based on percolation. In this model we imagine that the particles are ejected in random directions from a point source, and that they all slow to a stop in the same distance. In the spherical region where the particles stop, some will be close enough to touch. These touching particles stick together to form the aggregates we observe. If the particle density were large enough, percolating clusters would form. Under the right conditions one might preferentially observe these large clusters. The density correlations one measured would then be those within a percolating cluster. These correlations are known to have power-law behaviour (Kasteleyn and Fortuin 1969), and the exponent D is estimated (Stanley 1977) to lie near 1·8.

Table 3. Nominal D values for model systems.

Model	Field $\rho(r)$ (see equation (1))	$d = 2$	$d = 3$
Ising model (Brezin *et al* 1976)[a]	spin density	$\frac{7}{4}$	~1·96
Self-avoiding walk (McKenzie 1976)[b]	step density	~$\frac{4}{3}$	~$\frac{5}{3}$
Percolation (Stanley 1977)[a]	sites in percolating cluster	~1·8	~2

[a] D is taken to be equal to $2 - \eta$, using η values from this reference.
[b] D is taken to be equal to $1/\nu$ from this reference.

   While our results are consistent with the above power-law picture, they are not good enough to rule out other interpretations. In fact, we have found a simple model with no critical exponent which fits our data nearly as well as the percolation model does. This model treats the aggregates as simple two-dimensional random walks. We assumed that the random walks consisted of nearest-neighbour steps on a hypothetical square lattice, and that the number of steps was not.fixed, but exponentially distributed. The average density of points at a distance r from some step of such a walk is given by the modified Bessel function $K_0(2r/R)$ (Feller 1966), where R is the RMS average distance between any two steps (for r and R much larger than the lattice spacing). As with any two-dimensional random walk, the density has a logarithmic divergence for small distance. At large distances the density of these walks varies as $r^{-1/2} \exp(-2r/R)$. The result is that the apparent exponent D changes very slowly from 2 at small r to 1·5, before dropping rapidly at large r as a result of the exponential. We find (figure 3(*b*)) that our data fit this random-walk model nearly as well as they fit the power law.

   The above discussion shows that the correlations we have observed need not imply a critical exponent. Of the two models we have proposed, though, the percolation model with its critical exponent seems the more plausible. In any case, it appears from our data that these random particle aggregates have density distributions of a general and long-range form. It is likely that these correlations can be explained by means of a simple model such as the ones we have proposed. Or it may be that these correlations are of a new type not previously seen. An experiment with larger samples and better statistics would settle the question. A wider range of materials and conditions should be studied to explore the generality of our finding.

References

Abarbanel H D I 1978 *FNAL preprint*
Brézin E, LeGuillou J C and Zinn-Justin J 1976 *Phase Transitions and Critical Phenomena* eds C Domb and
    M S Green (New York: Academic)
Duneau M, Iagolnitzer D and Souillard B 1974 *Commun. Math. Phys.* **35** 307
Feller W 1966 *An Introduction to Probability Theory and Its Application* (New York: Wiley)
Fisher M E 1967 *Rep. Prog. Phys.* **30** 615
—— 1974 *Rev. Mod. Phys.* **46** 597
Granqvist C G and Buhrman R A 1976 *J. Appl. Phys.* **47** 2200
Harris A B, Lubensky T C and Chen J-H 1976 *Phys. Rev. Lett.* **36** 415
Hausdorff F 1919 *Ann. Math.* **79** 157, 179
Jenkins G W and Watts D G 1968 *Spectral Analaysis and Its Applications* (San Francisco: Holden-Day)
Kasteleyn P W and Fortuin C M 1969 *J. Phys. Soc. Japan Suppl.* **26** 11
Mandelbrot B B 1977 *Fractals: Form Chance and Dimension* (San Francisco: Freeman)
McKenzie D S 1976 *Phys. Rep.* **27** 35
Nelkin M 1975 *Phys. Rev.* A **11** 1737
Stanley H E 1977 *J. Phys. A: Math. Gen.* **10** L211
Stanley H E, Birgeneau R J, Reynolds P J and Nicoll J F 1976 *J. Phys. C: Solid St. Phys.* **9** L553
Wada N 1967 *Japan J. Appl. Phys.* **6** 553